Does ENSO Force the PNA?

DAVID M. STRAUS AND J. SHUKLA

Center for Ocean–Land–Atmosphere Studies, Calverton, Maryland

(Manuscript received 29 May 2001, in final form 21 February 2002)

ABSTRACT

The primary effect of El Niño–Southern Oscillation (ENSO) sea surface temperature (SST) anomalies is to force distinct midlatitude patterns, and not only to modify the probability of the internal variability patterns [such as the Pacific–North American (PNA) pattern of Wallace and Gutzler]. Both the spatial structure and probability distribution of the external ENSO pattern are distinct from the PNA pattern. Ensemble general circulation model (GCM) integrations for 30 winters have been analyzed in the Pacific–North America region. These winters span the recent period of 1981/82 through 1998/99, plus 12 earlier winters; the entire dataset includes six El Niño (warm) and seven La Niña (cold) events. The ensemble size is nine simulations. Empirical orthogonal function (EOF) analysis is carried out for all GCMs and observed seasonal means, for the GCM ensemble means, and for the GCM deviations about the ensemble means. EOF-1 of the GCM 200-hPa height (Z) ensemble mean agrees well with EOF-1 of all GCM seasonal means, and with the pattern that optimally filters out the internal variability. This ENSO pattern agrees with EOF-1 of reanalysis data, although the latter is modified in the Atlantic sector by the presence of the North Atlantic Oscillation pattern. An internal pattern closely resembling the PNA pattern is obtained here from reanalyses as EOF-2 of Z for 37 normal winters (winters that are neither warm nor cold). The GCM version of the PNA pattern can be seen in EOF-2 of the deviation of the GCM means about the ensemble mean, EOF-3 of all GCM seasonal means, and EOF-2 of a GCM integration made with climatologically varying SST.

Projections of all GCM seasonal means in a low-dimensional space indicate a segregation of the warm winter seasonal means from those of normal winters along the axis representing the external pattern. There is no support for the hypothesis that the probability distribution functions (pdfs) of internal and external variability are similar.

There is clear evidence of shifts in the probability of occurrence of internal patterns in warm and cold winters compared to normal winters. This has been analyzed in terms of only one set of characteristic patterns based on all winters. A more detailed investigation of the dependence of internal variability on SST forcing requires a larger ensemble size.

Intraseasonal variability is examined by projecting all individual pentad means on both the ENSO pattern and the PNA pattern (represented by the EOF-1 and EOF-3 of all seasonal means). For five out of the six warm winters, the pdfs of the time series of the coefficient of the ENSO pattern are shifted significantly toward more positive values, with very little probability of having a negative coefficient. For the cold events, the ENSO pattern has greater variability than the PNA pattern. The pdf of the projections of pentads on the seasonal mean anomaly for the same year are sharply peaked.

The GCM tropical heating maps show similar patterns for cold and normal winters, while the warm winter pattern is clearly different, especially along the equator. The heating anomalies have larger magnitude in warm than in cold winters. Linearity of the leading ensemble mean principal component (PC) with respect to the Niño-3 index of SST is seen only for positive SST anomalies. When Niño-3 is replaced by heating averaged over the central Pacific, there is a consistent relationship between the ENSO PCs and both positive and negative heating. Niño-3 depends on heating in a linear way for positive heating anomalies, but is independent of heating for negative anomalies.

1. Introduction

There is a fundamental debate in the literature as to how the dominant patterns characterizing the midlatitude response to tropical sea surface temperature (SST) anomalies are related to the preferred internal variability patterns of the atmosphere. The internal variability is due to the nonlinear nature of the atmospheric circulation, and gives rise to an unpredictable component of seasonal means (Lorenz 1964). The debate specifically centers around the question of whether the midlatitude seasonal mean circulation associated with El Niño–Southern Oscillation (ENSO) related tropical SST anomalies can be understood primarily in terms of a shift in the classic Pacific–North American (PNA) teleconnection pattern of internal variability of Wallace and Gutzler (1981), or whether such SST anomalies generate a fundamentally distinct forced response pattern.

One school of thought has taken the position that ENSO SST forcing can selectively amplify natural forms of internal variability but cannot generate new structures (Molteni et al. 1993; Lau 1997; Bladé 1999;

Corresponding author address: David M. Straus, Center for Ocean–Land–Atmosphere Studies, 4041 Powder Mill Rd., Suite 302, Calverton, MD 20705.
E-mail: straus@cola.iges.org

Palmer 1999). For example, Lau (1997) states that ''internal dynamics makes substantial contributions to the low-frequency variability of the midlatitude atmosphere. The insertion of . . . boundary forcing . . . apparently enhances the frequency of occurrence of such internal atmospheric modes during SST episodes . . . .'' Bladé (1999) also concludes, ''anomalous boundary forcing . . . alters the distribution of variance among *preexisting* preferred modes of low frequency variability but does not generate new structures'' (italics in original).

One of the main purposes of this article is to offer support for an alternative hypothesis: The response to external forcing can lead to patterns distinct from those associated with internal variability, and in particular, the dominant pattern associated with the El Niño–related tropical external forcing is quite distinct from dominant internal modes, including the PNA pattern. We define the distinction between internal and external variability in terms of sets of multiple realizations (or ensembles) of atmospheric states associated with the same boundary forcing. Here, the external variability is defined as the variability of the ensemble mean over the entire set of boundary forcings. This corresponds to the potentially predictable component, or signal, associated with the boundary forcing. Similarly, the internal variability is defined in terms of the set of deviations about the ensemble mean, and thus describes the variability of seasonal means in the presence of specified boundary forcing. Internal variability is ultimately due to nonlinear chaotic dynamics and is essentially unpredictable. These definitions hold in the limit of an infinite ensemble size; for finite ensembles, only estimates of the predictable or unpredictable components are accessible.

The lack of sensitivity of earlier general circulation models (GCMs) to tropical SSTs led to the impression that the dominant midlatitude pattern forced by tropical SST anomalies resembled the PNA pattern (e.g., see the study of Lau and Nath 1994.) Recently, Straus and Shukla (2000; hereafter S2000) presented an analysis of winter ensemble simulations of a realistic GCM in conjunction with observations (reanalyses) that emphasized that *the ENSO and PNA patterns are distinct*. This paper not only uses a larger GCM database simulation, but also presents a new and detailed investigation of the probability distribution of internal and externally forced seasonal mean atmospheric states.

From a purely observational point of view, the difference between the PNA and the leading ENSO height patterns has been commented on extensively in the literature (see, e.g., Barnston and Livezey 1987; Livezey and Mo 1987; Robertson and Ghil 1999), yet the structural difference between the PNA and ENSO patterns is still not always appreciated by researchers, as in the case of Hannachi (2001).

The ENSO phenomenon involves large SST anomalies in the eastern tropical Pacific, which lead to substantial anomalies in evaporation and the reorganization of cumulus convection throughout the Pacific, providing a deep anomalous tropical heat source. This in turn produces a Rossby wave response, which emanates into the extratropics, particularly the Pacific–North America region (see, e.g., Horel and Wallace 1981; Hoskins and Karoly 1981; Simmons 1982; Sardeshmukh and Hoskins 1988; Straus and Shukla 1997). The associated shifts in transient fluxes of heat and momentum are also known to play a crucial role in determining the time mean extratropical response (Held et al. 1989; Ting and Held 1990; Hoerling and Ting 1994). Figure 1 shows the dominant seasonal mean anomaly patterns observed at upper levels associated with warm and cold episodes.

The PNA pattern was originally described in monthly mean data of the midlevel height field by Wallace and Gutzler (1981) and has been studied extensively since then (see, e.g., Barnston and Livezey 1987; Cheng et al. 1995). A depiction of this pattern in seasonal means is also given in Fig. 1. This pattern is remarkably robust in nature and emerges from differing types of diagnostics, such as teleconnection calculations and rotated empirical orthogonal function analysis. The PNA pattern shows remarkably little sensitivity to the choice of which particular winters from the available record are used, so that it appears to have its origin in internal midlatitude dynamics. Further evidence of this was provided by Lau (1981), who shows that the PNA pattern is a dominant mode of variability in GCM simulations in which the lower boundary conditions followed a prescribed annual cycle with no interannual anomalies whatever. Since the ENSO tropical SST anomalies are very strong in some winters and not present at all in others, the very robustness of the PNA pattern in the observations argues strongly that it is an internal variability pattern. For the ensemble GCM runs with interannually varying SSTs that are discussed in this paper, empirical orthogonal function (EOF) analyses of the deviations of seasonal means about the ensemble mean produce a pattern very similar to the PNA pattern. This EOF pattern is also obtained from the seasonal means of an integration with climatologically varying SSTs. These results, to be discussed in this paper, further support the view that the PNA pattern is characteristic of internal dynamics.

In this paper, we will present an approach that is designed to systematically distinguish between the predictable response to ENSO-related SST anomalies and the internal variability, and to estimate the associated probability distributions from GCM ensemble experiments. Since the EOF methodology used tends to mask the difference between the response to El Niño (warm) winters and La Niña (cold) winters, we thus present additional analyses in sections 3 and 7, to focus on those differences.

It is important to understand that the structure of internal variability can, and in general does, depend on SST forcing. This dependence has been the subject of a number of recent papers (Kumar et al. 2000; Sar-

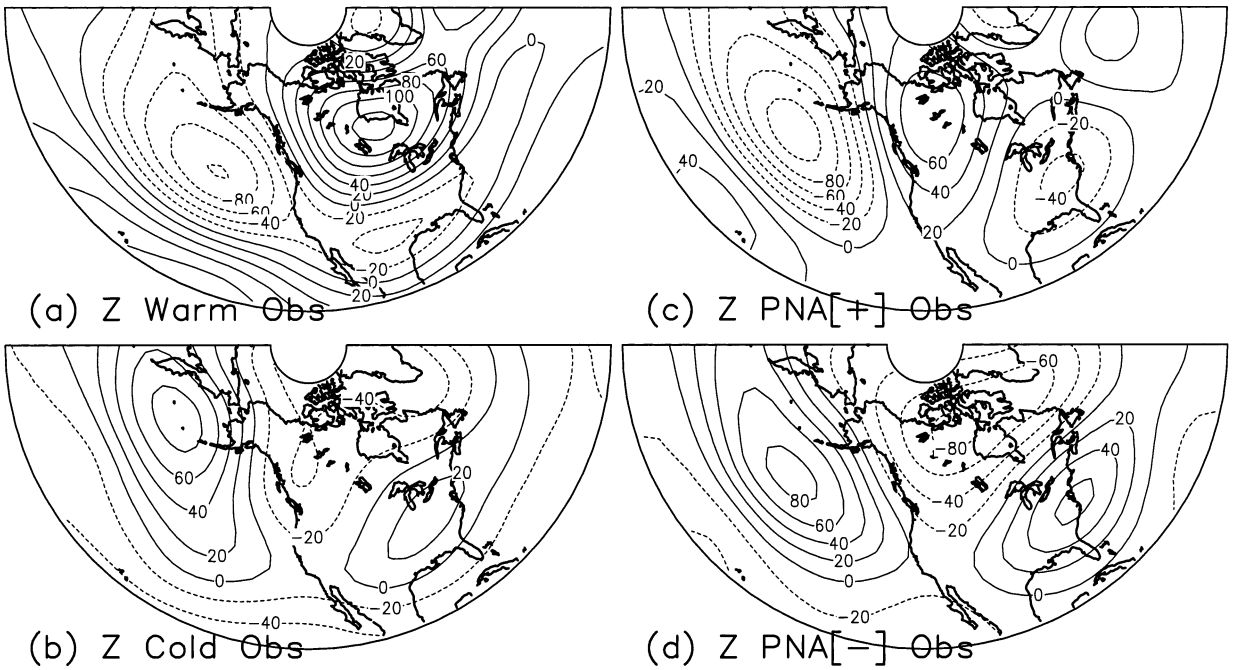

FIG. 1. The 200-hPa height field obtained from (a) ENSO warm minus normal winter seasonal mean composites and (b) ENSO cold minus normal winter seasonal composites, from NCEP–NCAR reanalyses. The 200-hPa height field difference of the (c) PNA(+) and normal phases and (d) PNA(−) and normal phases obtained from normal winter seasonal means from NCEP–NCAR reanalyses using the compositing technique of Wallace and Gutzler (1981). Contour interval is 20 m.

deshmukh et al. 2000; Schubert et al. 2001). Thus, strictly speaking, it is not valid to refer to internal variability simply as ''noise,'' as this would imply that it is independent of the forcing. The important physical point is that the changes in the mean state forced by SSTs lead to modifications in the character of the intraseasonal fluctuations. The internal variability in seasonal means is to a large extent a statistical residue of such fluctuations (Schubert et al. 2001).

The distinction between internal and external modes of variability in this paper is based on seasonal means obtained from multiple simulations of a GCM in which the boundary forcing (SST) is controlled, as in S2000. We also make use of reanalysis data. A brief description of the data, both from reanalyses (also called observations) and from the Center for Ocean–Land–Atmosphere Studies (COLA) GCM, is given in section 2. Section 3 will introduce and define the observed and simulated PNA and ENSO patterns from a simple analysis. An EOF-based approach to defining the leading external (signal) and internal patterns of variability obtained from the GCM ensemble experiments will be presented in section 4. In section 5 we use a phase-space representation of the seasonal means from the simulations to define probability distribution functions associated with internal and external variability. Intraseasonal variability during normal winters and strong ENSO events will be considered in section 6. In section 7 we will return to the question of how El Niños differ from La Niñas. A discussion is given in section 8, and we offer a summary and conclusions in section 9.

2. Data and definitions

We make use of both reanalyses (also called observations) and integrations of the general circulation model of the Center for Ocean–Land–Atmosphere Studies. The reanalyses are obtained from National Centers for Environmental Prediction–National Center for Atmospheric Research (NCEP–NCAR) for the winters of 1949/50 through 1998/99 (Kalnay et al. 1996). Here, winter is defined as the 90-day season starting on 20 December.[1] Each winter is defined (with respect to ENSO) as ''warm'' (the Niño-3 index is above 1.0 standard deviation), ''cold'' (the Niño-3 index is below −1.0 standard deviation), or ''normal'' (all other winters). Niño-3 is defined as the SST anomaly averaged over the area 5°S–5°N, 150°–90°W, and is obtained from the data of Smith et al. (1996). There are 7 cold events, 6 warm events, and 37 normal years (see Table 1).

The GCM integrations were made in conjunction with the Dynamical Seasonal Prediction project (DSP), which encompassed ensemble seasonal integrations with a number of GCMs. Here we utilize the results

[1] The start date of 20 December was the earliest date, given the initial conditions of all the integrations, for which we could conveniently align the pentads used in section 6.

TABLE 1. Chronological list of warm and cold ENSO winters, defined as those winters for which the Niño-3 index is above 1.0 (below −1.0) std dev where the statistics of the Niño-3 index are based on the 50 winters of 1949/50–1998/99.

Warm	Niño-3	Cold	Niño-3
1957/58	1.44	1949/50	−1.69
1972/73	1.38	1955/56	−1.07
1982/83	3.02	1967/68	−1.55
1986/87	1.28	1970/71	−1.59
1991/92	1.59	1973/74	−1.57
1997/98	2.86	1975/76	−1.47
		1988/89	−1.26

from the COLA GCM (see also Shukla et al. 2000a,b; S2000). Each ensemble consists of nine simulations initialized from analyses during mid-December of a particular winter, and runs through the end of March using the evolving weekly SSTs that were observed for that winter. (For details of the COLA GCM, initial conditions, and SST, see Shukla et al. 2000b). In S2000, such ensembles were created for the 16 winters of 1981/82 through 1996/97. In this paper we augment those simulations with ones made for the more recent winters of 1997/98 and 1998/99, as well as an additional 12 (nonconsecutive) earlier winters that sampled warm and cold ENSO episodes: 1949/50, 1955/56, 1957/58, 1959/60, 1965/66, 1967/68, 1968/69, 1970/71, 1972/73, 1973/74, 1975/76, 1976/77. The dataset consisting of all 30 yr is referred to as DSP30. The list of warm and cold years of Table 1 also applies to the GCM data. Note that there are 17 normal winters for the GCM.

A further reference integration of the COLA GCM was made for 38 yr using climatologically varying SSTs (i.e., with SST following the annual cycle but having no interannual variability). The set of 38 winters from this integration is referred to as the CliSST dataset.

3. PNA and ENSO anomalies: A simple approach

In order to define the ENSO and PNA patterns in the seasonal mean 200-hPa height field, we present a simple analysis. The warm (cold) ENSO anomaly is defined as the difference of the average over all warm (cold) winters and the average for normal winters. The observed results shown in Fig. 1 are based on the 50 winters of 1949/50–1998/99, encompassing 37 normal winters and the 6 warm and 7 cold winters given in Table 1. The GCM results shown in Fig. 2 use all simulated seasonal means, with the same 6 warm and 7 cold winters, but with 17 normal winters available. The warm and cold anomalies are depicted for the observations in Figs. 1a and 1b, and for the GCM in Figs. 2a and 2b. We also show a version of the classic PNA pattern. This was obtained by compositing the seasonal mean 200-hPa height field based on the PNA index originally defined by Wallace and Gutzler (1981). The index was applied only to the *normal* winter seasonal means. Since only normal winters were used, primarily internal variability

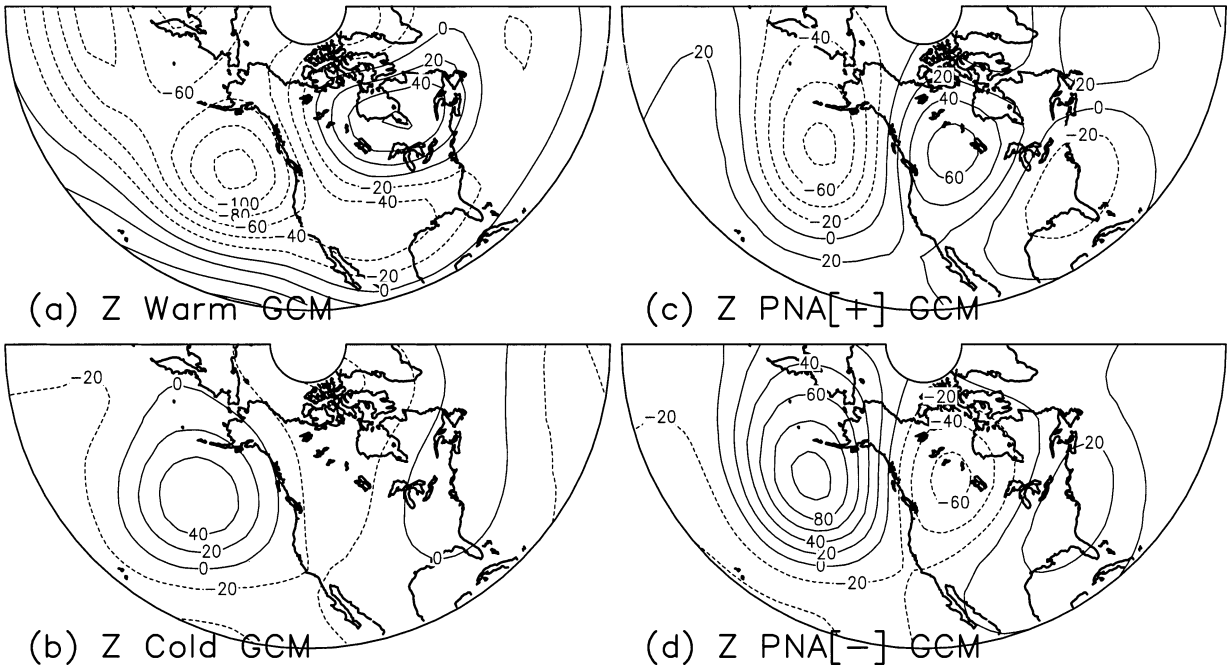

FIG. 2. The 200-hPa height field obtained from (a) ENSO warm minus normal winter seasonal mean composites and (b) ENSO cold minus normal winter seasonal composites, from the COLA GCM ensemble means. The 200-hPa height field difference of the (c) PNA(+) and normal phases and (d) PNA(−) and normal phases obtained from normal winter seasonal means from the COLA GCM using the compositing technique of Wallace and Gutzler (1981). Contour interval is 20 m.

(with respect to ENSO) contributes to these patterns. The PNA(+) [PNA(−)] pattern is the difference between the winter seasonal means averaged over all normal winters when the PNA index is above 1.0 standard deviation (below −1.0 standard deviation) and the climatology for the normal winters. The PNA patterns for the observations are shown in Figs. 1c and 1d, and for the GCM in Figs. 2c and 2d.

It is quite clear that the composite warm ENSO anomaly is quite distinct from the PNA(+) anomaly in both the observations and the GCM. While both anomalies might be described as ''wave trains,'' the placement and orientation of the high over North America is dramatically different, leading to a dominantly meridional gradient of height over much of North America in the ENSO circulation as compared to a much weaker and more zonally oriented height gradient in the PNA(+). The warm ENSO anomaly implies a significant shift in the geostrophic wind, with the extension of the subtropical Pacific jet toward the southwest coast of North America. No such extension is associated with the PNA pattern. Both the spatial structure and amplitude of the GCM patterns are in generally good agreement with the observations. Discrepancies include the center over northeastern Canada in the warm ENSO anomaly (the GCM is too weak), and the cold ENSO anomaly (the GCM is again too weak). An important conclusion is that the ENSO cold and PNA(−) anomalies are much more similar to each other than their warm and PNA(+) counterparts. This holds for both the GCM and the observations.

From this simple analysis it appears that the ENSO warm response is distinct from one component of natural variability as defined from the PNA index, but that the ENSO cold response may not be. Hoerling et al. (1997, 2001) have already emphasized the difference between the warm and cold anomalies. Their results are similar to those shown in Fig. 1. The analysis presented in Fig. 1 has limitations. The method of abstracting the ENSO signal in observations is prone to contamination by internal variability; only a fairly small number of atmospheric states enters the warm or cold composite, and each state making up that composite has an SST anomaly that is different in detailed structure both in the Tropics and globally, even if the value of the Niño-3 index is similar. (Kumar and Hoerling 1997 have also emphasized this point.) Furthermore, efforts to obtain internal variability patterns other than the PNA pattern, in order to construct a consistent basis set of natural variability patterns, are confounded by the fact that such teleconnection patterns are neither orthogonal in space nor independent in time.

4. External and internal GCM EOFs

In order to consistently isolate the atmospheric internal variability from the response to SST (external variability), it is necessary to have multiple realizations of the atmosphere for the same SST forcing. Since nature does not provide us with this, it is necessary to use GCM simulations. The concern for consistent estimates of forced vs internal variability was the driving force behind the DSP project, which is briefly described in section 2. With an ensemble of atmospheric GCM states obtained for each SST forcing, the set of ensemble means can be used to estimate the SST-forced signal, while the deviations about the ensemble mean can be used to estimate the internal variability. This estimate can be compared to that obtained from the CliSST integrations.

In order to correctly distinguish between forced patterns and those due to internal dynamics, it will be helpful to address the dependence of the character of the internal variability on SST. This paper will discuss this dependence primarily in the context of a single set of characteristic patterns derived below. This set of patterns is derived from deviations about the ensemble means from *all* seasons, making no distinction based on SST forcing. We will briefly compare this set of characteristic internal patterns to those derived using normal SST (with respect to ENSO) winters only. To go beyond this and derive distinct sets of characteristic internal patterns for different SST forcings requires an ensemble size 1 order of magnitude larger than used here (see Sardeshmukh et al. 2000). As we will discuss, this will place some limits on the scope of questions we can answer.

a. EOF approach

We compute the EOFs of the GCM ensemble mean 200-hPa height field to obtain a set of patterns that characterizes the variability of the SST-forced response. The domain used in this and all subsequent EOF calculations is the region 20°–80°N, 150°E–30°W. Each of the EOF patterns that is presented is dimensional (with units of meters) and is associated with a time series (principal component), which has unit variance.[2]

Similarly, EOFs are calculated from the set of deviations of seasonal means about their respective ensemble mean to obtain characteristic patterns of internal variability. As stated above, we have also computed the EOFs of the ensemble deviations based only on the 17 normal GCM winters. These external and internal variability patterns are *not* orthogonal (nor are their respective time series uncorrelated), since they arise from distinct EOF analyses. This makes it impossible to uniquely decompose a field into external and internal components. Thus we have also computed the EOFs of all raw seasonal means and have identified patterns from

[2] The spherical geometry is accomodated by weighting all input fields by the square root of the cosine of latitude, assuring that the variances are correctly weighted. The square root weighting is divided out before plotting the patterns.

TABLE 2. Percentage of variance explained by leading EOFs for seasonal mean 200-hPa height for GCM datasets: Ens avg refers to ensemble average, all sea refers to all-season means, ens dev to deviations about the ensemble average. Obs30 consists of the observations for the same winters as DSP30. ObsNorm consists of the 37 winters that were not warm or cold events during the period 1949/50–1998/99. Pattern identifiers are given in bold lettering: AO = combination of Arctic Oscillation and NAO, EAO = combination of ENSO and NAO, PNA and ENSO, as in text.

Dataset	EOF-1	EOF-2	EOF-3
DSP30 ens avg	**ENSO 44**	21	11
DSP30 all sea	**ENSO 30**	**AO 20**	**PNA 15**
DSP30 ens dev	**AO 36**	**PNA 14**	14
CliSST	**AO 50**	**PNA 16**	11
Obs30	**EAO 41**	**PNA 23**	10
ObsNorm	**AO 34**	**PNA 20**	15

this analysis that are close to particular patterns of forced or internal variability.

The four leading EOF patterns from all four calculations are given systematically in the appendix (Figs. A1–A4), while the associated percentage of variance explained is given in Table 2 (and also in the figures). The leading EOF of the ensemble means is nearly identical to the warm-ENSO pattern of Figs. 1a and 2a, and is identified simply as the ENSO pattern. The composite cold event seen in Figs. 1b and 2b is not captured by a single EOF, a matter we will discuss later in the paper. Comparison of the ensemble deviation EOFs from the full GCM set (Fig. A2) and the normal years (Fig. A3) shows that the patterns are nearly identical, indicating that this basis set of internal variability patterns is a reasonable one to use. In both cases, EOF-2 is nearly identical to the PNA pattern identified from the simple analysis given in section 3. The leading EOF of the all-season EOFs (Fig. A4) is very similar, but not identical to, the ENSO pattern identified by EOF-1 of the ensemble means, while EOF-3 of the all-season EOFs is very similar to the PNA pattern of both GCM ensemble deviation calculations. In the following analysis, we will use EOF-1 and EOF-3 as *approximate* representations of the ENSO and PNA patterns, respectively. EOF-2 of the all-season analysis is not present in either the ensemble mean or ensemble deviation analyses and is interpreted as a hemispheric representation of the Arctic Oscillation, or AO (Thompson and Wallace 2000). This pattern seems to be neither purely forced by global SSTs nor purely independent of them, a point to which we will return.

b. External variability

Figures 3a and 3b give various representations of the ENSO signal. EOF-1 of the ensemble means explains a substantial fraction of the total variance (44%) and dominates the EOF spectrum (see Table 2). The EOF-1 pattern is nearly identical to that shown in S2000. In principle, the leading EOF of the ensemble means represents the predictable component of the response to the *global* SST anomalies that occurred during the period. However, the high correlation (0.85) between the time series (principal component) of the leading EOF and the time series of Niño-3 indicates that the eastern tropical

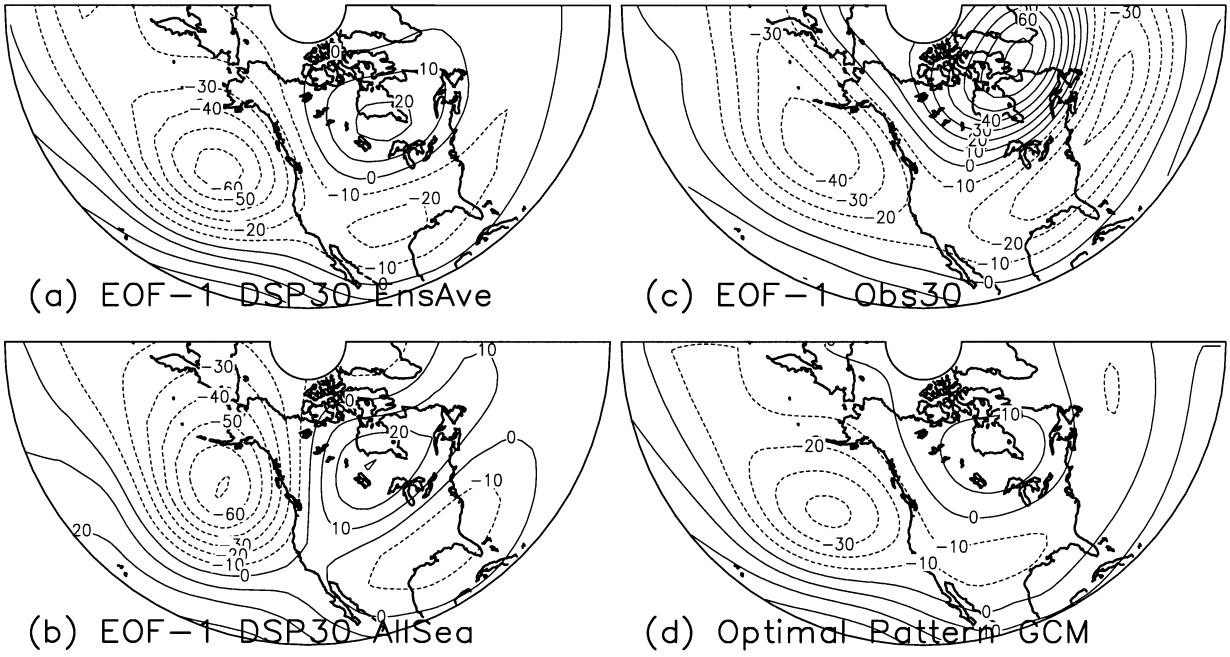

FIG. 3. EOFs of seasonal mean 200-hPa height. The corresponding time series are normalized to have unit variance: (a) EOF-1 for ensemble mean from DSP30, (b) EOF-1 for all-season means from DSP30, (c) EOF-1 for 30 observed winters corresponding to DSP30, (d) optimal pattern for DSP30 (see text for explanation). Contour interval is 10 m.

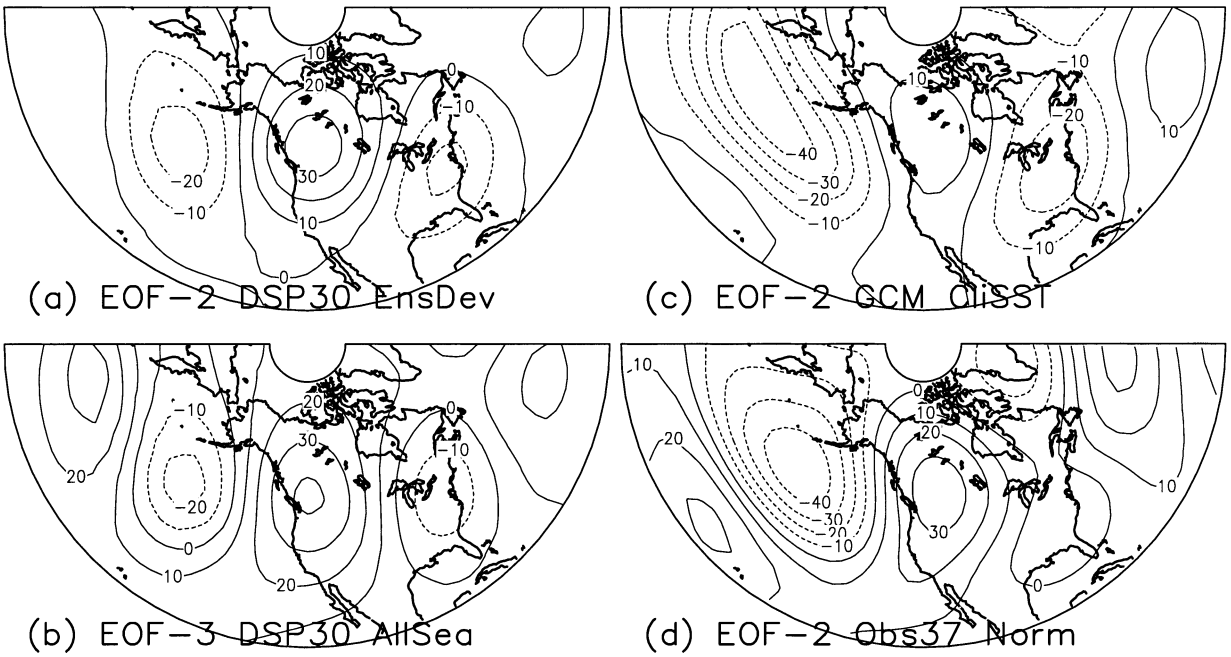

FIG. 4. EOFs of seasonal mean 200-hPa height. The corresponding time series are normalized to have unit variance: (a) EOF-2 for deviation from ensemble mean from DSP30, (b) EOF-3 for all-season means from DSP30, (c) EOF-2 for all-season means of CliSST GCM integration, (d) EOF-2 for seasonal mean 200-hPa height from 37 normal observed winters. Contour interval is 10 m.

Pacific (ENSO) SST anomalies dominate in defining this signal. The strong similarity in pattern between the results shown here and those of S2000 indicates a robustness to the period chosen. Furthermore, very similar patterns have been derived from analyses that specifically link the height field to the tropical Pacific SST anomalies, as shown in S2000.

Since the estimate of the response to SST forcing obtained from the ensemble means is still contaminated by chaotic internal variability because of the finite ensemble size (Rowell et al. 1995; Shukla et al. 2000b), we have applied a technique to the DSP30 dataset that is designed to maximize the ''signal-to-noise'' ratio. This technique, discussed in Venzke et al. (1999), determines a pattern whose associated time series has the maximum ensemble mean variability with respect to its intraensemble variability. The so-called leading optimal pattern given in Fig. 3d. It is very similar to the leading EOF of the ensemble means.

The leading EOF obtained from *observed* seasonal means for the winters corresponding to the DSP30 dataset is shown in Fig. 3c. This EOF also dominates in terms of explained variance (see Table 2). While differences between GCM and observed patterns are due both to the lack of an ensemble in nature and to errors in the GCM, an important difference is a consistent eastward extension into the Atlantic Ocean in the observations compared to the absence of such in the GCM. This is a clear sign of the North Atlantic Oscillation (NAO; see Rogers 1984), which for the GCM at least is an element of internal variability, and so has been correctly filtered out by the ensemble means.

Figure 3b shows the leading EOF of *all* 270 seasonal means from the DSP30 dataset. It strongly resembles the corresponding EOF of the ensemble means, with only minor differences.

c. Internal variability

Patterns of internal variability can be defined from EOF analysis of the deviations about the ensemble means in the DSP30 dataset, as discussed in section 4a, and independently from the long integration using climatologically varying SSTs (the CliSST dataset). These are shown in Fig. 4. The second EOF of the ensemble deviations resembles the PNA pattern of the COLA GCM (cf. Fig. 4a with Fig. 2c). It strongly resembles EOF-3 from the all-season analysis (Fig. 4b). EOF-2 from the CliSST run (shown in Fig. 4c) has a stronger and more extensive Pacific Ocean weighting and a weaker western Canadian weighting, but is otherwise similar.

In order to help interpret these GCM patterns in terms of observed ones, we have also computed the leading EOFs from the 37 winters of the NCEP–NCAR reanalyses for which the Niño-3 index was within one standard deviation from the long-term average, the normal winters of section 2. This is shown in Fig. 4d. The comparison of GCM results to observations here is of course very crude, since the observed atmosphere was

subject to a different SST boundary condition for each of the winters considered. While the leading EOF of observations (not shown) contains elements of the NAO and the Arctic Oscillation, the EOF-2 pattern strongly resembles the PNA pattern of Wallace and Gutzler (1981). It also has a strong degree of similarity with the GCM internal variability patterns shown in Figs. 4a–c.

The GCM version of the PNA pattern shown in Figs. 4a–c is clearly quite distinct from the SST-forced ENSO pattern shown in Figs. 3a, 3b, and 3d. In the ENSO pattern, the high over North America is shifted nearly 40° of longitude to the east compared to the PNA pattern. This results in the primarily north–south height gradient in the ENSO pattern being replaced with an east–west gradient in the PNA pattern. This difference is emphasized by the EOF expansion based on all GCM seasonal means. EOF-1 and EOF-3 (Figs. 3b and 4b) are estimates of the ENSO and PNA patterns that are *both orthogonal in space and independent in time*.

The second external EOF (EOF-2 from the seasonal ensemble mean; see Fig. A1) also resembles the internal patterns shown in Figs. 4a–c. The centers are close to those in Fig. 4a, but the magnitude of the continental centers are relatively much weaker. This EOF can be thought of as one correction to the dominant EOF necessary to describe the external, SST-forced signal in DSP30. Its resemblance to the PNA pattern suggests that it might provide the explanation for the warm/cold asymmetry seen in Fig. 1. We will take up this point in section 7.

5. GCM states in phase space

The notion that external tropical SST forcing only changes the probability of the atmosphere residing in one of its internal modes can be tested in the appropriate phase space. In such a phase space, the probability distribution for warm ENSO events would be shifted (as compared to normal winters) along the axis (or axes) representing the internal modes, but *not* along the axis (or axes) representing the external modes. In fact, under this hypothesis there should be no way of separating the two types of modes.

The purpose of this section is to present such phase-space plots. The all-season analysis introduced in the previous section was motivated by the need for a set of orthogonal and independent patterns representing external and internal variability. In this set of EOFs, EOF-1 represents the (warm) ENSO signal, EOF-3 is the PNA internal pattern, and EOF-2 (the AO) is a mixed forced/internal pattern. By representing the seasonal mean atmospheric states as points in this three-dimensional space, which captures 65% of the space–time variance, we derive two-dimensional probability distribution functions (pdfs) in planes of this space. The focus will then be on the shifts of the pdfs between warm, normal, and cold years along various EOF directions.

Figure 5 shows a depiction of the projections of all-season means on the plane defined by EOF-1 and EOF-3, the ENSO and PNA patterns, respectively. Each solid circle represents the position of a single GCM seasonal mean in this coordinate system. The colors (red, green, blue) denote winters considered to be (warm, normal, cold) with respect to Niño-3, as described in section 2. Figure 6 shows a similar plot of the ensemble means projected onto the same plane. The warm winters occupy a region in phase space distinct from both the normal and cold winters, with a much larger component of EOF-1 (ENSO signal). This is particularly true for the ensemble means. There is also a more subtle distinction between the normal and cold winters, with the cold winters favoring the second quadrant.

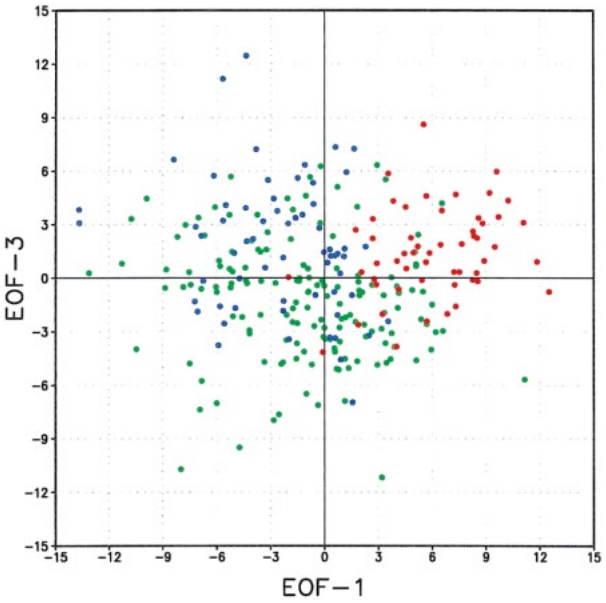

FIG. 5. Coordinates of all seasonal mean 200-hPa height fields from DSP30 in the EOF-1/EOF-3 plane. EOFs are from DSP30 all-season means. The (red, green, blue) circles correspond to (warm, normal, cold) winters for all seasonal means. EOF patterns used to define the coordinates are normalized to unit sum of squares, coordinate labels on the x and y axes are in units of 100 m.

An alternate method of depicting these projections is to estimate the smooth pdfs based on the individual projections. These are shown for both the EOF-2/EOF-1 planes and the EOF-3/EOF-2 planes in Fig. 7.[3] In this figure, the warm winter pdf (red contours), the cold winter pdf (blue contours), and the normal winter pdf (black contours) are compared pairwise for each plane. The distinction between warm/cold and warm/normal distributions is very strong for both the EOF-2/EOF-1 and EOF-3/EOF-2 planes. The subtle distinction between the cold and normal winter projections in the

[3] A bivariate kernal density estimator (Silverman 1986) was used to estimate the pdf for each season separately, and the pdfs for the warm, normal, and cold seasons were obtained as averages of the individual season pdfs.

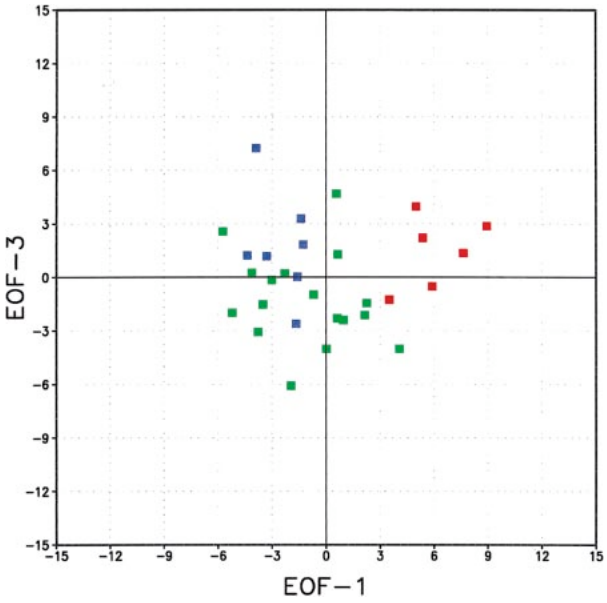

FIG. 6. Coordinates of ensemble seasonal mean 200-hPa height fields from DSP30 in the EOF-1/EOF-3 plane. EOFs are from DSP30 all-season means. The (red, green, blue) squares correspond to (warm, normal, cold) winters for ensemble means. EOF patterns used to define the coordinates are normalized to unit sum of squares, coordinate labels on the *x* and *y* axes are in units of 100 m.

EOF-3/EOF-1 plane apparent in Figs. 5 and 6 is made more clear in this depiction.

The significant difference between warm and cold years in Fig. 7d is a distinct shift of the pdfs along the ENSO (EOF-1) axis. The warm years also show the same shift along the EOF-1 axis with respect to the normal years in Fig. 7e. The cold years show no shift along this axis with respect to normal years. As we will discuss later, higher-order signal EOFs are needed to describe the cold year signals.

The warm year pdf shows some overlap with the cold and normal year pdfs in Fig. 7d–f. This in part reflects the fact that the pattern associated with EOF-1 only approximately represents the leading signal EOF (cf. Figs. A1a and A4a), and the fact that since the El Niño SST anomalies vary from event to event, the signal associated with each event will in general not have the same decomposition in terms of the multiple signal EOFs. The inter–El Niño variability (also referred to as the ''different flavors of ENSO'') is an important research topic in seasonal-to-interannual research. [Note, however, that Kumar and Hoerling (1997) argue that the observed inter–El Niño variability is caused by chaotic variability superimposed on a single external pattern.]

The spread of the warm year pdf along the ENSO-signal (EOF-1) axis raises the legitimate question of whether this ENSO signal is itself a pattern of internal variability during warm years. In other words, do various ensemble members during a warm year differ from each other primarily by the strength of the ENSO signal, or is the variability within warm year ensembles dominated by other patterns? The answer to this question would involve large ensembles for warm years only, and cannot be answered definitively (even for the COLA GCM) by the data available here. However, we can get a simple, if crude, estimate by plotting the deviations about the ensemble means for all warm years only in planes of the EOF-1 to EOF-3 phase space, and looking for a clear tendency of the points to line up along the EOF-1 axis as opposed to orthogonal to it. We have done this (not shown), and our preliminary results do not strongly argue that the ENSO signal is an internal mode of variability during warm events. However, a more definitive answer will come from larger ensembles in work that is under way.

There are some interesting distinctions between warm, normal, and cold years in terms of their projections onto EOF-2 (the AO pattern) and EOF-3 (the PNA pattern). While normal and cold years project approximately equally on both signs of the AO pattern, the warm years tend to have more positive values of the AO, indicating that for the COLA GCM the pattern (shown in Fig. A4b) is enhanced during warm events. With respect to the PNA pattern represented by EOF-2, its positive phase is more strongly excited by both warm and cold winters compared to normal winters. We cannot offer an explanation of this, but we can compare the SST dependence of the PNA pattern implicit in Figs. 7d,e with that reported by Renshaw et al. (1998, their Fig. 6). These authors report a shift in the PNA pdf toward more negative values (stronger low in the North Pacific) during cold events for both their GCM and observations. This agrees with our Figure 7f. However, for warm winters Renshaw et al. obtain little change in the observed PNA pdf, and a positive shift of their GCM. From Figure 7e it is clear that the COLA GCM indicates a negative shift in the PNA pdf for warm events. The indications are either that neither model is realistic in this sense, or that sampling error is an issue. Model dependence of internal variability was also reported by Kumar et al. (2000).

These results give little support for the hypothesis that the warm states preferentially occupy certain subregions of those parts of phase space occupied in the absence of ENSO forcing. The warm distributions show significant displacements from the cold and normal distributions along an axis unambiguously associated with the SST forced signal.

6. Intraseasonal variability

While the anomalous upper-level height response to strong ENSO SST anomalies is well defined in the seasonal mean, it is not clear whether these anomalies are statistical residues of intraseasonal fluctuations that have a very different character, or are in some sense noticeably present for much of the season. This intuitive question may not always be answerable, since both or neither

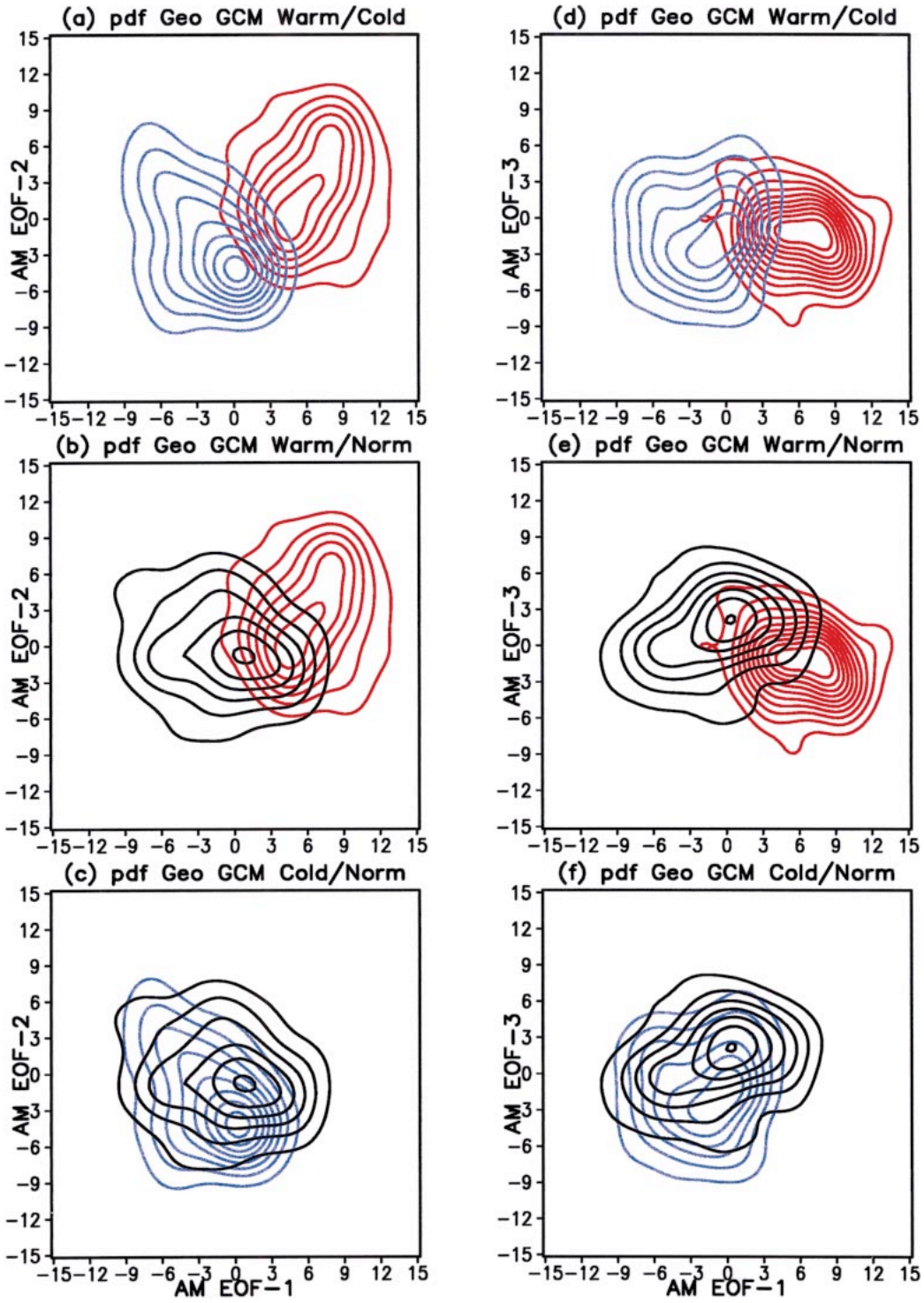

FIG. 7. Two-dimensional pdfs for all-season mean 200-hPa height fields from DSP30 warm (red), normal (black), and cold (blue) winters in the (a)–(c) EOF-2/EOF-1 and (d)–(f) EOF-1/EOF-3 plane: (a), (d) warm and cold winters; (b), (e) warm and normal winters; (c), (f) cold and normal winters. All-season EOF patterns used to generate the coordinates have been normalized to unit sum of squares, x and y coordinates are in units of 100 m.

possibility may be operative in individual cases. It does, however, suggest that the determination of the intraseasonal variability of the external pattern might prove insightful. We examine this question by assessing the degree of variability of the ENSO and PNA patterns contained within individual 5-day (pentad) means.

One-dimensional pdfs of the projections of individual pentads on the basis set consisting of the (all season) EOF-1 and EOF-3 (the ENSO forced and PNA internal patterns) used in the previous section are presented in Figs. 8 and 9. The smooth probability distribution functions[4] of ENSO and PNA projections of all (162) GCM pentads for the warm winter of 1982/83 are shown in Fig. 8a, with the ENSO pdf given by the black solid curve and the PNA pdf by the black dashed curve. There is a very clear separation between the pdfs. While the PNA pattern projection is slightly more likely to be negative than positive, the ENSO pattern has a very small likelihood of having a negative sign. *The pdfs are significantly different at the* 99% *level*.[5] Similar plots for all six warm winters are given in the other panels in Fig. 8, in which the value of Niño-3 for each winter is given in parentheses. The ENSO pattern projection is much more (less) likely to be positive (negative) than the PNA pattern projection in all winters except 1957/58, for which the difference in pdfs is more subtle. In all cases, the black dashed and solid pdfs are significantly different at the 99% level.

Since any individual warm event anomaly (obtained by the ensemble mean) is composed of more than just the leading signal EOF, this analysis may underestimate the sharpness of the pdfs for individual years. Hence, we also present the projections of all pentads for a given year on the seasonal ensemble mean anomaly for that year. These pdfs, given by the red curves in Fig. 8, indicate clearly that for each of the six warm events, an individual pentad is very unlikely to have the opposite pattern to the signal associated with that event's SST anomaly.

Corresponding plots for six of the cold events are presented in Fig. 9. While the ENSO and PNA pdfs are still different at the 99% level in four of the winters (1967/68, 1970/71, 1973/74, and 1975/76), the nature of the distinction is that the ENSO signal pdfs are generally wider than the PNA pdfs, indicating greater variability. This is in part a reflection of the fact that the single ENSO signal pattern, approximately represented by EOF-1, is a better match for warm events than for cold events, and the fact that intraseasonal variability in cold events is believed to be enhanced (see, e.g., Chen and van den Dool 1997). Note that the distributions of the pentad projections on the anomalies for each year (given by the blue curves) are generally more sharply peaked than the ENSO-signal projection pdfs.

7. Linearity of the ENSO response

The differences in patterns between the observed seasonal mean anomalies for strong warm and strong cold events (Figs. 1 and 2) indicate that the ENSO response depends on the sign of the SST anomaly (Hoerling et al. 1997). This is seen in both GCM and observational results.

How can we reconcile the difference between warm and cold event composites with the strong dominance of the leading EOF of the ensemble mean in terms of explained variance? While warm event signals are approximately captured with only the leading signal EOF, cold event signals have larger weights for the higher-order signal modes (EOFs). Consider the contribution of the second ensemble mean EOF pattern (shown in Fig. A1b). Scatterplots of both PC-1 and PC-2 (time series of EOF-1 and EOF-2) for the GCM ensemble mean height versus Niño-3 are shown in Fig. 10, where the red, green, and blue dots again indicate warm, normal, and cold years. While there is a fairly strong relationship between Niño-3 and the value of PC-1 for positive Niño-3, the value of PC-1 for negative Niño-3 is nearly independent of the value of Niño-3. (The straight lines represent linear fits, done separately for positive and negative Niño-3.) There is no apparent relationship between the value of PC-2 and Niño-3 for positive Niño-3, but Fig. 10b does suggest a relationship for negative Niño-3. For example, five out of the seven cold years have a negative value for PC-2.

Figure 11 shows scatterplots of PC-1 and PC-2 not against an SST-derived variable, but an index that describes the vertically integrated GCM nonadiabatic heating in the tropical Pacific. Specifically, the index is the vertically integrated heating averaged over the area 5°S–5°N, 180°–300°E, normalized to unit variance. Again, the red, green, and blue colors indicate the warm, normal, and cold years. There clearly is a relationship between heating and PC-1 for both positive and negative values of the heating, although whether this relationship has a nonlinear component is not clear given the present number of ensemble means. PC-2 shows little relationship with heating for the positive heating index, but again a relationship with negative heating index is apparent. Figure 11c shows a scatterplot of the heating against Niño-3. While the strong expected relationship shows up for positive values of Niño-3, the heating anomalies are unrelated to Niño-3 for negative values since a broad range of negative heating anomalies is associated with Niño-3 anomalies in a very small range. Our Fig. 11c is comparable to Fig. 11 of Hoerling et al. (2001), who plot tropical precipitation versus the first principle component of tropical SST.

[4] A univariate kernal density estimator (Silverman 1986) was used to estimate all pdfs.

[5] The statistical significance of the difference between pdfs is assessed with Kuiper's statistic, as discussed in Press et al. (1992).

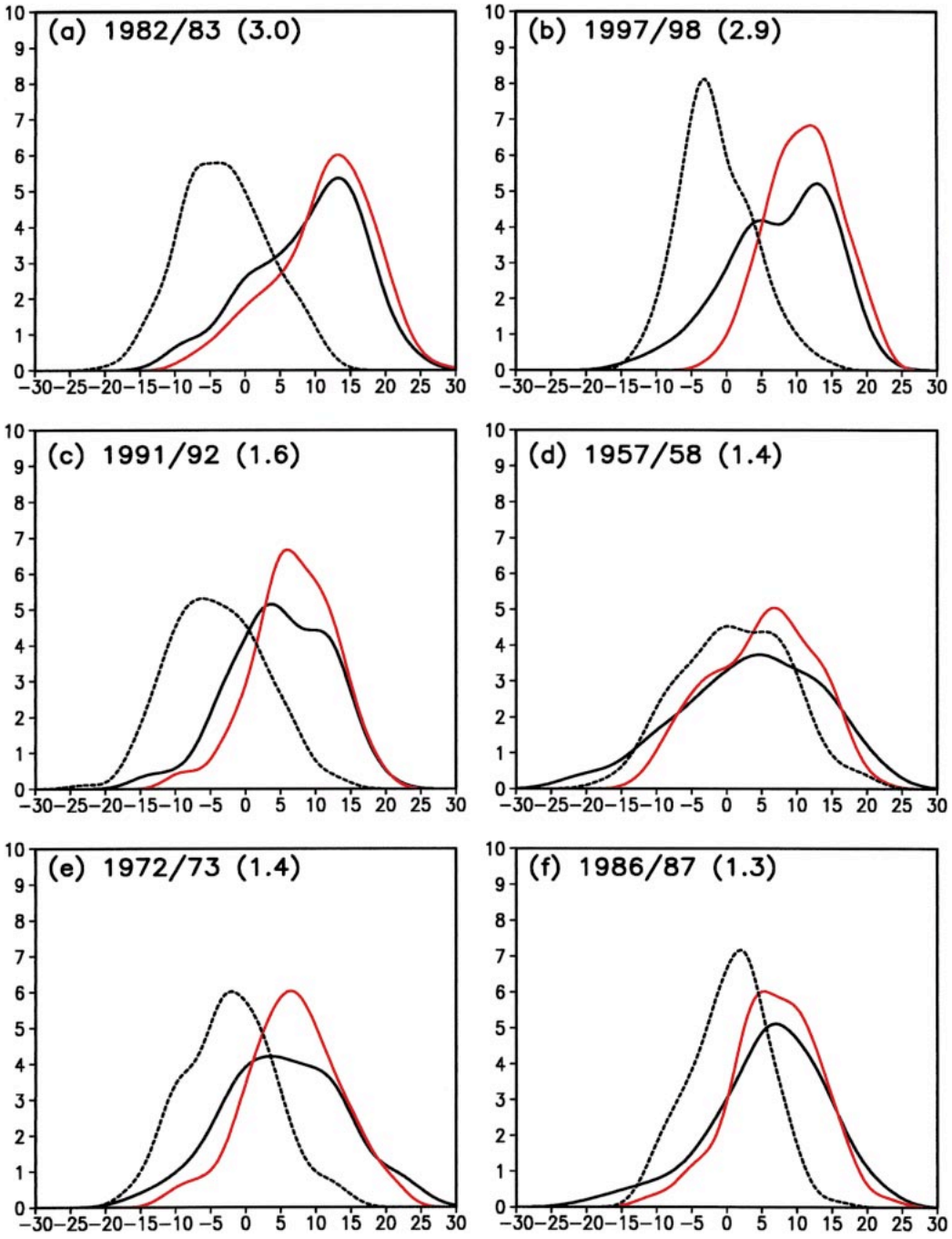

FIG. 8. Probability distribution function of the projections of all pentad means of 200-hPa *Z* (from DSP30) onto the ENSO pattern (solid black curves) and the PNA pattern (dotted black curves). ENSO (PNA) pattern is given by EOF-1 (EOF-3) from all DSP30 seasonal means. Red curves give the projections of all pentad means on the seasonal ensemble mean anomaly for the particular winter. Winters are labelled. Corresponding values of Niño-3 are given in parentheses.

These results indicate that the second EOF of the ensemble means helps to explain the distinction between the responses to warm and cold events, although higher-order signal EOFs are also needed. More research with a larger sample size is needed to further study this question. It is clear from Fig. 11 that heating is a more appropriate variable on which to base a linear statistical relationship than is SST. The distinction between warm and cold events (for the GCM) is related to the smaller magnitude of the diabatic heating anomalies in the eastern tropical Pacific. The linear relationship suggested by Fig. 11a indicates a weaker EOF-

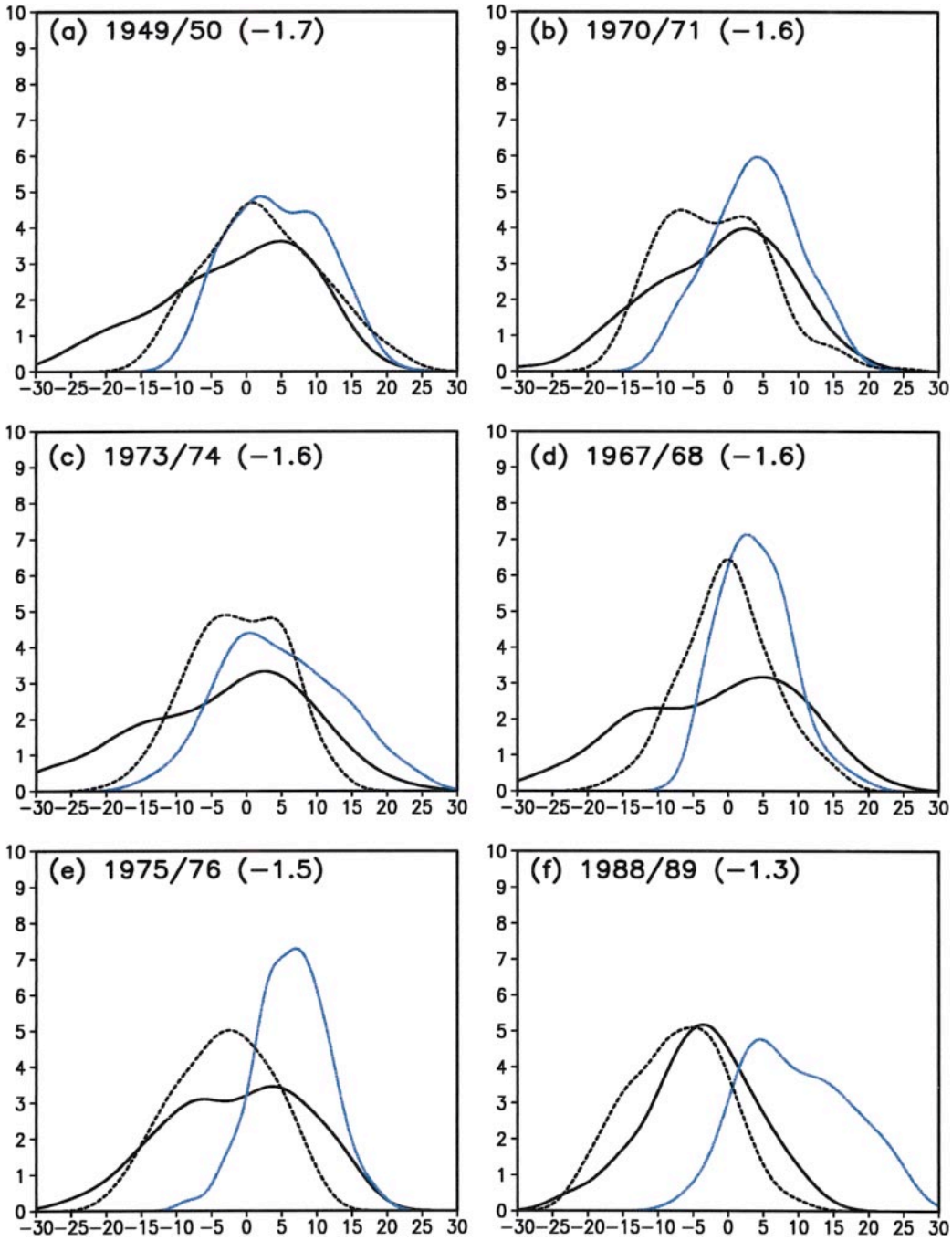

FIG. 9. As in Fig. 8, but for individual cold winters. Blue curves give the projections of all pentad means on the seasonal ensemble mean anomaly for the particular winter.

1 response in cold events compared to warm events, so that the total cold event response would be more susceptible to influence by other factors, including internal variability patterns.

Warm events are characterized not only by a stronger heating anomaly than cold events, but also by more of a change in the geographical structure of the heating from the normal configuration. Maps of the geographical structure of the vertically integrated (ensemble-seasonal mean) heating in DSP30, as well as the warm and cold anomalies, are shown in Figs. 12 and 13. The cold event heating pattern has the same broad structure as the normal pattern, with the difference mostly due to a westward shift of 15° in the equatorial boundary between heating and cooling for cold events, and somewhat weaker heating west of this. In stark contrast, the

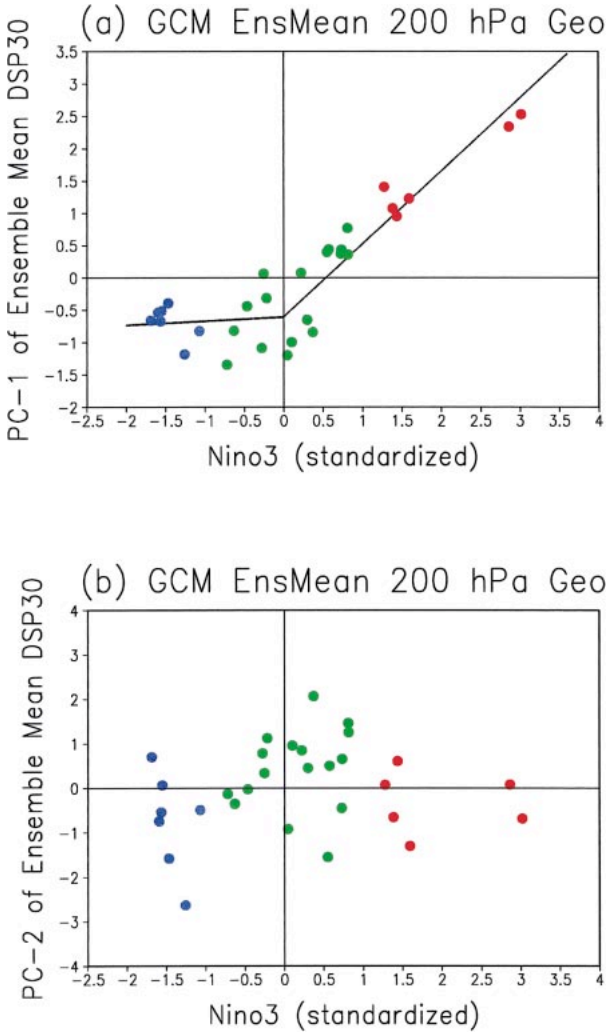

FIG. 10. Scatterplot of (a) leading principal component (PC-1) and (b) PC-2 of ensemble mean seasonal mean 200-hPa height for DSP30 against Niño-3 index. PCs and Niño-3 have been normalized to unit variance. The red, green, and blue colors correspond to warm, normal, and cold winters, respectively.

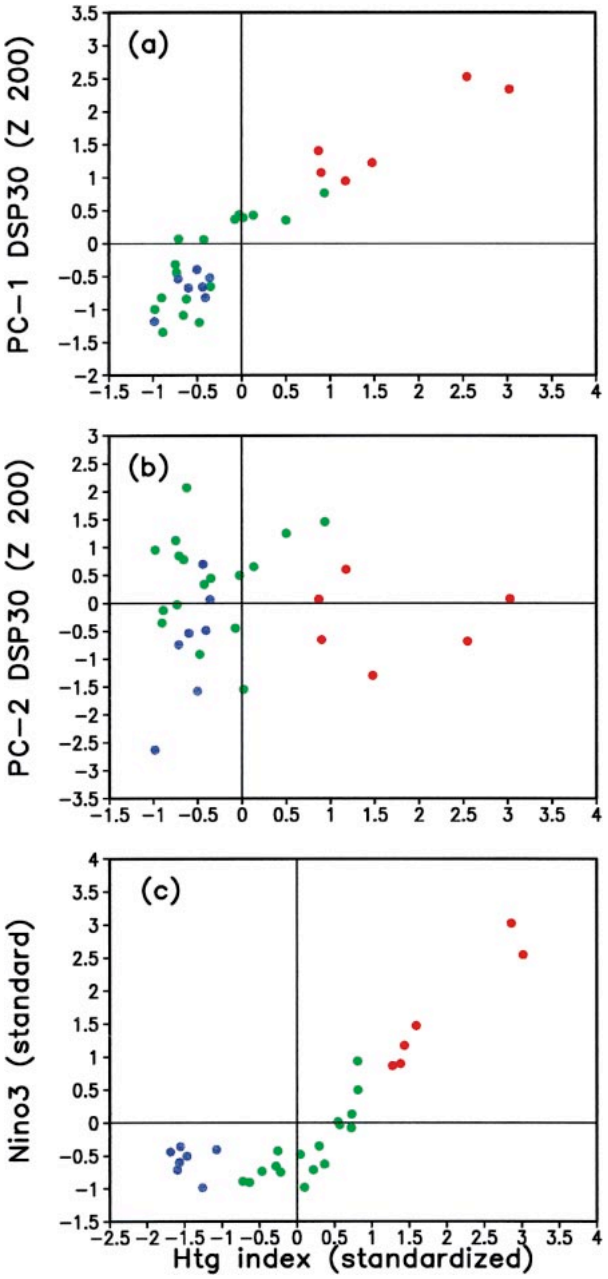

FIG. 11. Scatterplot of (a) leading principal component (PC-1) and (b) PC-2 of ensemble mean seasonal mean 200-hPa height for DSP30 against heating index, defined as the vertically integrated GCM heating averaged over the area 5°S–5°N, 180°–300°E. PCs and heating index have been normalized to unit variance. (c) Scatterplot of Niño-3 against the heating index. The red, green, and blue colors correspond to warm, normal, and cold winters, respectively.

warm event heating has a totally different equatorial structure, replacing the normal cooling east of about 175°W with heating. The most intense La Niña cooling anomalies are less than half as strong as the largest El Niño heating anomalies. The behavior of these GCM-derived heating fields has been qualitatively verified by comparison to the vertically integrated heating equivalent from observational estimates of precipitation given by the Global Precipitation Climatology Project (Huffman et al. 1997), and the Climate Prediction Center Merged Analysis of Precipitation (Xie and Arkin 1997) for the 12 overlap winters of 1981/82 through 1998/99. The precipitation anomalies during warm and cold events from four GCMs shown in Hoerling et al. (2001) also tend to support our results.

8. Discussion

Since the distinction between the signal and the internal variability in our framework depends on the availability of multiple atmospheric realizations of the COLA GCM in the presence of identical boundary forcing,

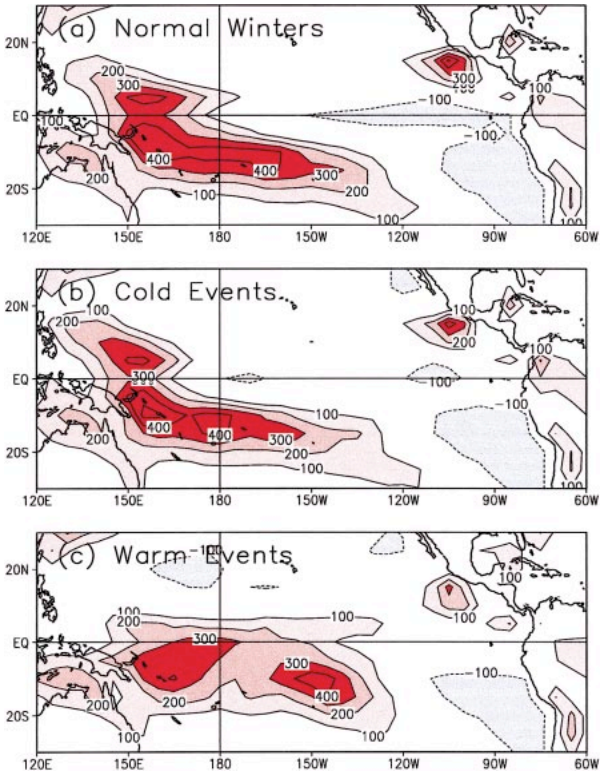

FIG. 12. Seasonal mean vertically integrated heating from DSP30 ensemble means averaged over all: (a) normal winters, (b) cold winters, (c) warm winters. Contour interval is 100 W m^{-2}. The zero contour is suppressed.

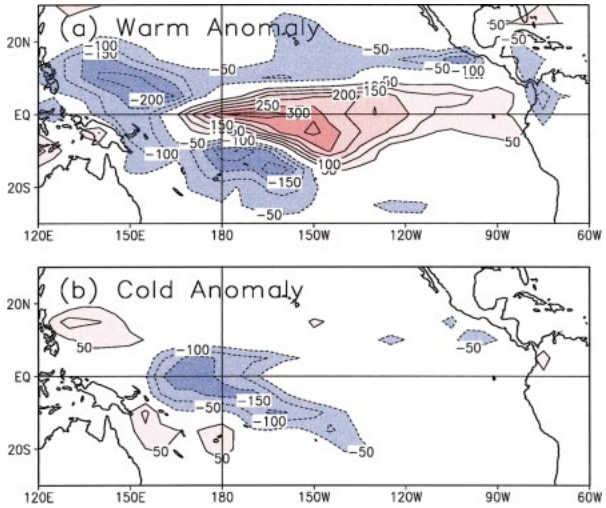

FIG. 13. Seasonal mean vertically integrated heating from DSP30 ensemble means: (a) warm winter minus normal winter average, (b) cold winter minus normal winter average. Contour interval is 100 W m^{-2}. The zero contour is suppressed.

many of the results of this paper depend on the properties of the COLA GCM. From Shukla et al. (2000a), it is clear that within the group of six models presented, the ENSO-forced response of the COLA GCM is above average (although not the strongest). This tendency is in part reflected by the similarity between the leading EOFs of the ensemble means and all-season means (see Figs. A1 and A4, respectively). It is not possible to determine which of the GCMs presented in Shukla et al. (2000a) is the most like nature in responding to El Niño forcing. However, we note that the most weakly responding model in this study, the Goddard Space Flight Center (GSFC) Earth Observing System (GEOS-2) GCM (Chang et al. 2000), has been replaced with a GCM that shows a considerably larger response (S. Schubert and M. Suarez 2000, personal communication).

It is also clear that the dependence of the internal variability distribution on the forcing may be dependent on the characteristics of the GCM. The shifts in the pdf of the PNA pattern with SST seen in the COLA GCM in Fig. 7 are different than the GCM results cited by Renshaw et al. (1998), and neither set agrees completely with the observations.

It is noteworthy that the set of characteristic patterns of internal variability for the COLA GCM, based on all available winters, is not changed when we remove both cold and warm winters. However, it may well be that warm (or cold) ENSO winters may have their own distinct set of characteristic internal variability patterns. Much larger ensembles are required to investigate this.

9. Summary and conclusions

The answer to the question posed in the title of this paper, does ENSO force the PNA, is ''no'' for warm ENSO SST forcing. For cold event SST forcing, the results of this paper are not conclusive.

The dominant SST-forced pattern associated with warm ENSO SST forcing is distinct from the venerable PNA pattern, which is an internal pattern. Our ability to predict (or simulate) the response to even strong tropical SST anomalies has an intrinsic limitation due to the presence of internal variability—those fluctuations in the seasonal mean which are due entirely to chaotic atmospheric dynamics. Over the PNA region, the (internal) PNA pattern bears some very superficial resemblance to the dominant midlatitude ENSO SST response pattern (e.g., they both involve the Aleutian low area); a resemblance that had previously inspired the hypothesis that the atmospheric response to ENSO consists of only a change in the probability of occurrence of a particular phase of internal patterns. This paper presents evidence that the response to ENSO warm events involves more than a change in the pdf of the PNA.

Ensemble GCM experiments, where each ensemble provides nine seasonal mean atmospheric states for a given observed SST anomaly, provide a method for sep-

arating the external (SST forced) and internal (chaotic) variability. The former can be studied from the ensemble mean, the latter from the deviation of each seasonal mean about the ensemble mean. Long integrations with climatologically varying SSTs have also been used for studying the internal variability. The analysis of such ensemble experiments with the COLA GCM for 30 winters has provided consistent estimates of both the ENSO SST-forced external patterns (from EOF and optimal filtering techniques) and consistent estimates of the patterns of internal variability, which are characteristic of the dataset as a whole.

The rejection of the hypothesis that the external and internal variability involve the same anomaly patterns but with a different probability is supported with the use of two-dimensional probability distribution functions (pdfs) of GCM seasonal means in a plane in phase space in which one axis can be identified with the strength of an external pattern, and the second axis with an internal pattern. In this plane, the warm event pdfs are dramatically shifted from the cold event and normal pdfs, especially along the external mode axis. This type of phase-space analysis further suggests a dependence of the probability of occurrence of internal patterns on the external forcing. For example, the PNA pdf is different in the warm, cold, and normal populations.

The behavior of the ENSO SST-forced and PNA patterns on intraseasonal timescales is also distinct, as seen from the one-dimensional pdfs of the projections of individual pentad (5-day) means on the two patterns. For all warm events, the ENSO and PNA pdfs are significantly different (at the 99% level); there is very low probability of finding a negative ENSO pattern (that is, one with sign opposite to the leading warm event seasonal mean response), while this probability is much higher for the corresponding PNA pdf.

While the leading ENSO patterns are derived from all ensemble means, it is primarily the warm events that are so well characterized by the leading signal EOF. The cold events give more weight to the higher order signal EOFs. What is the significance of the fact that the cold event composites from observations and the GCM resemble the PNA pattern? It is not clear whether the lack of strong heating anomalies during cold events means that the internal mode shifts dominate, or whether patterns such as the second signal EOF (which superficially resembles the PNA pattern) are involved. In the latter case, the PNA pattern might also be said to be a signal pattern, although a secondary one. More research is clearly needed.

The asymmetry between warm and cold event responses is seen in the dependence of the strength of the leading EOF of external variability on both the Niño-3 index and on an index that measures the total tropical Pacific heating. A relationship between SST anomalies and the strength of the ENSO pattern is present only for warm anomalies. In contrast, we see a consistent (nearly linear) relationship between the ENSO pattern strength and the heating for both warm and cold events. One factor in differentiating cold from warm responses is thus the weaker heating anomalies during cold events; another is the structure of the heating, which is quite different from normal only during warm events. The qualitative features of the GCM's heating are consistent with satellite-based precipitation estimates from post-1980 winters. The warm–cold asymmetry indicates more than one EOF of the ensemble mean is needed to explain both types of response, and it is seen that the second EOF of the ensemble means plays a modest role in cold events.

It is suggested here that weaker tropical heating anomalies in cold (as compared to warm) winters make it harder to extract the forced signal from the internal variability. Understanding the distinctive characteristics of internal variability for cold events only or warm events only requires generating very large ensembles. Such work is currently under way.

Acknowledgments. We are grateful for the helpful advice of T. DelSole, especially with the calculation of the optimal pattern. This work was supported by the National Science Foundation under Grant ATM-98-14295, the National Aeronautics and Space Administration under Grant NAG5-8202, and the National Oceanic and Atmospheric Administration under Grant NA96-GP0056.

APPENDIX

The Four Leading EOF Patterns

We show the four leading EOFs for each of four calculations based on the seasonal mean 200-hPa height from the GCM ensemble experiments that encompass 30 winters. The domain used is the region 20°–80°N, 150°E–30°W. Each of the EOF patterns that is presented is dimensional (with units of meters) and is associated with a time series (principal component) that has unit variance. The spherical geometry is accomodated by weighting all input fields by the square root of the cosine of latitude, assuring that the variances are correctly weighted. The square root weighting is divided out before plotting the patterns. Figure A1 shows the leading EOFs of the ensemble means. The percentage of spatially averaged temporal variance explained is given in each of the four panels. The leading EOFs of the deviations of the seasonal means about the ensemble means are shown in Fig. A2. Figure A3 shows the EOFs of the deviation of the seasonal means about the ensemble means, but is calculated using only data for the 17 normal winters, that is, for those GCM winters not listed in Table 1. The leading EOFs of all-season means is shown in Fig. A4.

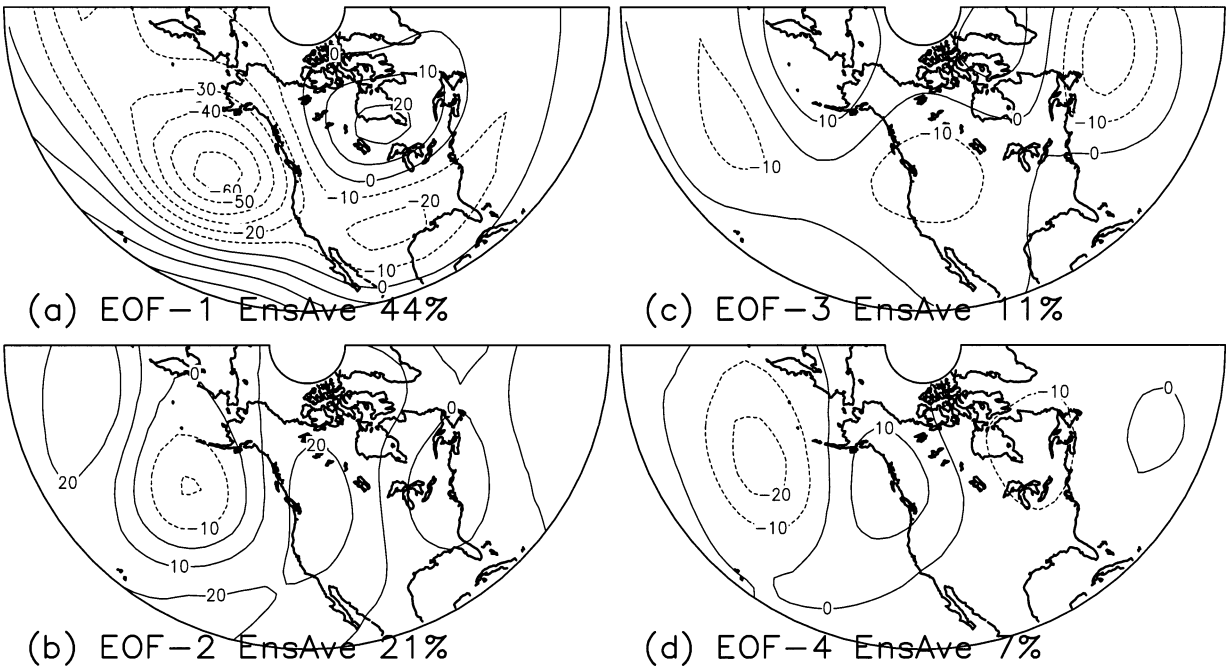

FIG. A1. EOFs of the ensemble seasonal means of 200-hPa height from the COLA GCM. Each pattern has a corresponding time series that has unit variance. The percentage variance explained by each EOF is indicated. (a)–(d) The four leading EOFs.

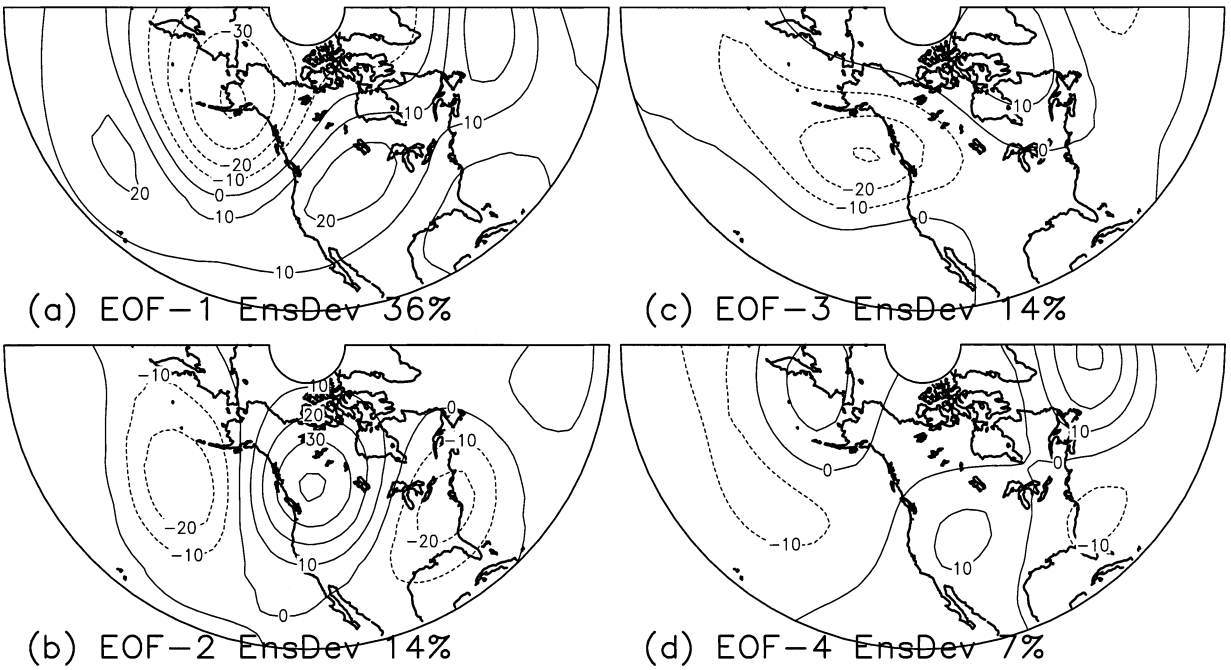

FIG. A2. EOFs of the deviations of seasonal means about the ensemble means of 200-hPa height from the COLA GCM. Each pattern has a corresponding time series that has unit variance. The percentage variance explained by each EOF is indicated. (a)–(d) The four leading EOFs.

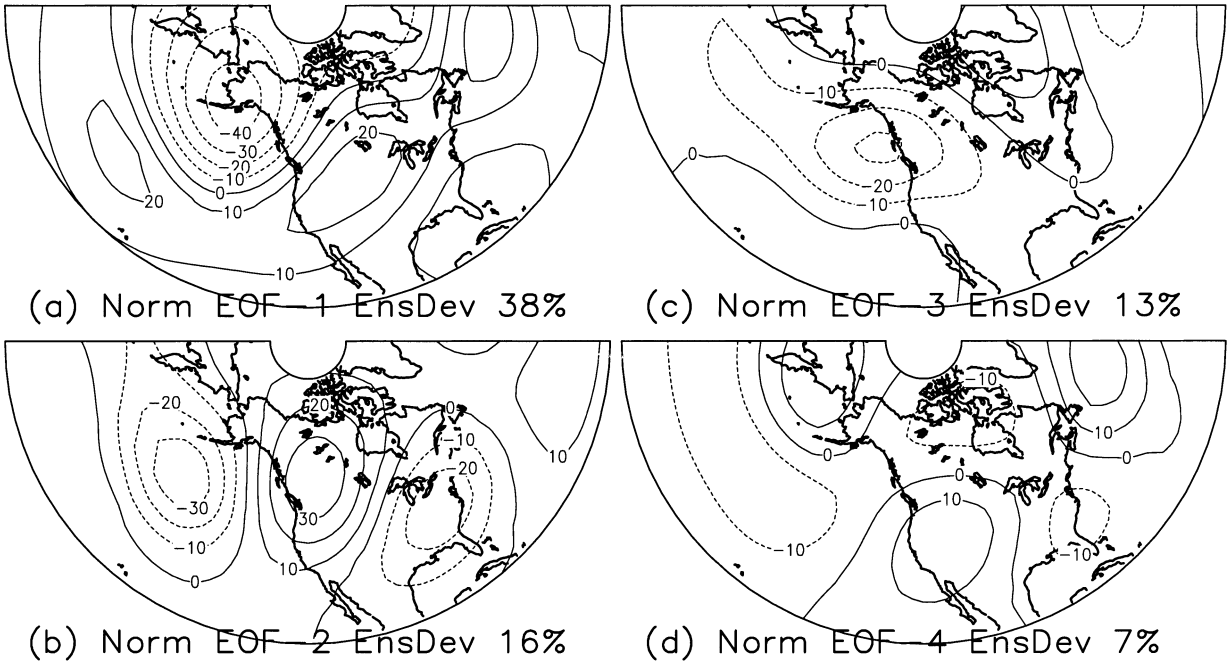

FIG. A3. As in Fig. A2, but based only on seasons for which the Niño-3 index is normal.

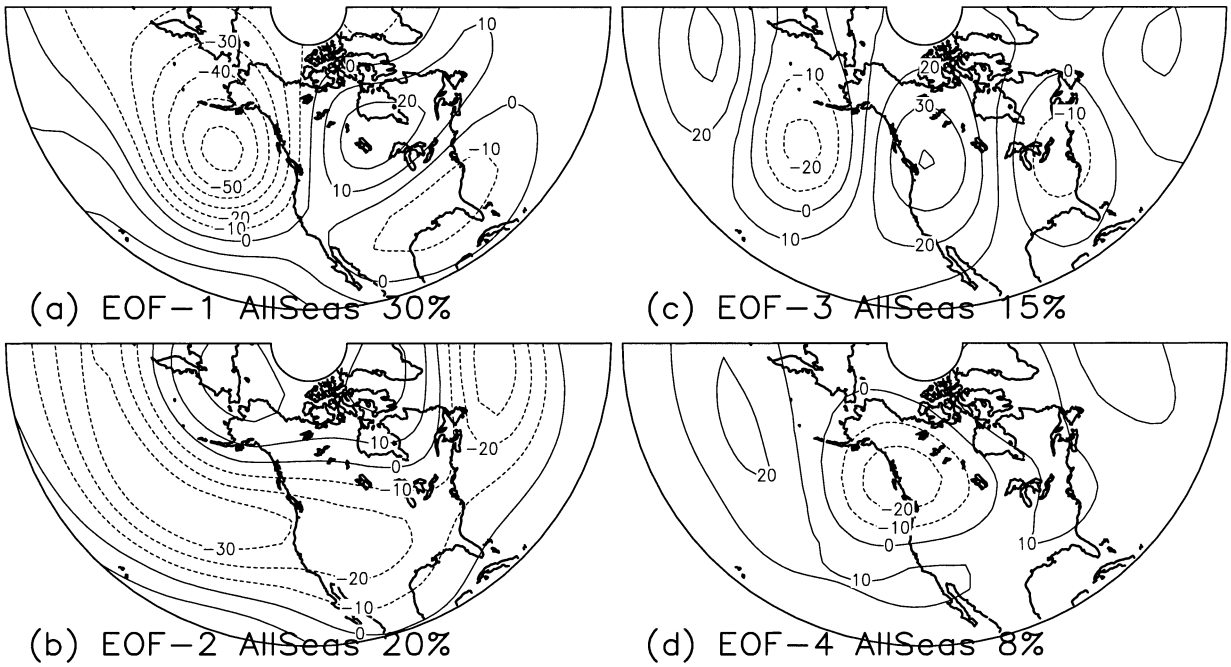

FIG. A4. EOFs of all seasonal means of 200-hPa height from the COLA GCM. Each pattern has a corresponding time series that has unit variance. The percentage variance explained by each EOF is indicated. (a)–(d) The four leading EOFs.

REFERENCES

Barnston, A. G., and R. E. Livezey, 1987: Classification, seasonality and persistence of low-frequency atmospheric circulation patterns. *Mon. Wea. Rev.,* **115,** 1083–1126.

Bladé, I., 1999: The influence of midlatitude ocean–atmosphere coupling on the low-frequency variability of a GCM. Part II: Interannual variability induced by tropical SST forcing. *J. Climate,* **12,** 21–45.

Chang, Y., S. D. Schubert, and M. J. Suarez, 2000: Boreal winter predictions with the GEOS-2 GCM: The role of boundary forcing and initial conditions. *Quart. J. Roy. Meteor. Soc.,* **126,** 2293–2323.

Chen, W. Y., and H. M. van den Dool, 1997: Asymmetric impact of tropical SST anomalies on atmospheric internal variability over the North Pacific. *J. Atmos. Sci.,* **54,** 725–740.

Cheng, X., G. Nitsche, and J. M. Wallace, 1995: Robustness of low-frequency circulation patterns derived from EOF and rotated EOF analyses. *J. Climate,* **8,** 1709–1720.

Hannachi, A., 2001: Toward a nonlinear classification of the atmospheric response to ENSO. *J. Climate,* **14,** 2138–2149.

Held, I. M., S. W. Lyons, and S. Nigam, 1989: Transients and the extratropical response to El Niño. *J. Atmos. Sci.,* **46,** 163–174.

Hoerling, M. P., and M. Ting, 1994: Organization of extratropical transients during El Niño. *J. Climate,* **7,** 745–766.

——, A. Kumar, and M. Zhong, 1997: El Niño, La Niña, and the nonlinearity of their teleconnections. *J. Climate,* **10,** 1769–1786.

——, ——, and T. Xu, 2001: Robustness of the nonlinear climate response to ENSO's extreme phases. *J. Climate,* **14,** 1277–1293.

Horel, J. D., and J. M. Wallace, 1981: Planetary scale phenomena associated with the Southern Oscillation. *Mon. Wea. Rev.,* **109,** 813–829.

Hoskins, B. J., and D. J. Karoly, 1981: The steady linear response of a spherical atmosphere to thermal and orographic forcing. *J. Atmos. Sci.,* **38,** 1179–1196.

Huffman, G. J., and Coauthors, 1997: The Global Precipitation Climatology Project (GPCP) combined precipitation dataset. *Bull. Amer. Meteor. Soc.,* **78,** 5–20.

Kalnay, E., and Coauthors, 1996: The NCEP/NCAR 40-Year Reanalysis Project. *Bull. Amer. Meteor. Soc.,* **77,** 437–471.

Kumar, A., and M. P. Hoerling, 1997: Interpretation and implications of observed inter–El Niño variability. *J. Climate,* **10,** 83–91.

——, A. G. Barnston, P. Peng, M. P. Hoerling, and L. Goddard, 2000: Changes in the spread of the variability of the seasonal mean atmospheric states associated with ENSO. *J. Climate,* **13,** 3139–3151.

Lau, N.-C., 1981: A diagnostic study of recurrent meteorological anomalies appearing in a 15-year simulation with a GFDL general circulation model. *Mon. Wea. Rev.,* **109,** 2287–2311.

——, 1997: Interactions between global SST anomalies and the midlatitude atmospheric circulation. *Bull. Amer. Meteor. Soc.,* **78,** 21–33.

——, and M. J. Nath, 1994: A modeling study of the relative roles of tropical and extratropical SST anomalies in the variability of the global atmosphere–ocean system. *J. Climate,* **7,** 1184–1207.

Livezey, R. E., and K. C. Mo, 1987: Tropical–extratropical teleconnections during the Northern Hemisphere winter. Part II: Relationships between monthly mean Northern Hemisphere circulation patterns and proxies for tropical convection. *Mon. Wea. Rev.,* **115,** 3115–3132.

Lorenz, E. N., 1964: The problem of deducing the climate from the governing equations. *Tellus,* **16,** 1–11.

Molteni, F., L. Ferranti, T. N. Palmer, and P. Viterbo, 1993: A dynamical interpretation of the global response to equatorial Pacific SST anomalies. *J. Climate,* **6,** 777–795.

Palmer, T. N., 1999: A nonlinear dynamical perspective on climate prediction. *J. Climate,* **12,** 575–591.

Press, W. H., S. A. Teukolsky, W. T. Vetterling, and B. P. Flannery, 1992: *Numerical Recipes in FORTRAN*. 2d ed. Cambridge University Press, 576 pp.

Renshaw, A. C., D. P. Rowell, and C. K. Folland, 1998: Wintertime low-frequency weather variability in the North Pacific–American sector 1949–93. *J. Climate,* **11,** 1073–1093.

Robertson, A. W., and M. Ghil, 1999: Large-scale weather regimes and local climate over the western United States. *J. Climate,* **12,** 1796–1813.

Rogers, J. C., 1984: The association between the North Atlantic Oscillation and the Southern Oscillation in the Northern Hemisphere. *Mon. Wea. Rev.,* **112,** 1999–2015.

Rowell, D. P., C. K. Folland, K. Maskell, and M. N. Ward, 1995: Variability in summer rainfall over tropical North Africa (1906–92): Observations and modelling. *Quart. J. Roy. Meteor. Soc.,* **121,** 669–704.

Sardeshmukh, P. D., and B. J. Hoskins, 1988: The generation of global rotational flow by steady idealized tropical divergence. *J. Atmos. Sci.,* **45,** 1228–1268.

——, G. P. Compo, and C. Penland, 2000: Changes of probability associated with El Niño. *J. Climate,* **13,** 4268–4286.

Schubert, S. D., M. J. Suarez, Y. Chang, and G. Branstator, 2001: The impact of ENSO on extratropical low-frequency noise in seasonal forecasts. *J. Climate,* **14,** 2351–2365.

Shukla, J., and Coauthors, 2000a: Dynamical seasonal prediction. *Bull. Amer. Meteor. Soc.,* **81,** 2593–2606.

——, D. A. Paolino, D. M. Straus, D. De Witt, M. Fennessy, J. L. Kinter, L. Marx, and R. Mo, 2000b: Dynamical seasonal prediction with the COLA atmospheric model. *Quart. J. Roy. Meteor. Soc.,* **126,** 2265–2291.

Silverman, B. W., 1986: *Density Estimation for Statistics and Data Analysis*. Chapman and Hall, 175 pp.

Simmons, A. J., 1982: The forcing of stationary wave motion by tropical diabatic heating. *Quart. J. Roy. Meteor. Soc.,* **108,** 503–514.

Smith, T. M., R. W. Reynolds, R. E. Livezey, and D. C. Stokes, 1996: Reconstruction of historical sea surface temperatures using empirical orthogonal functions. *J. Climate,* **9,** 1403–1420.

Straus, D. M., and J. Shukla, 1997: Variations of midlatitude transient dynamics associated with ENSO. *J. Atmos. Sci.,* **54,** 777–790.

——, and ——, 2000: Distinguishing between the SST-forced variability and internal variability in mid latitudes: Analysis of observations and GCM simulations. *Quart. J. Roy. Meteor. Soc.,* **126,** 2323–2350.

Thompson, D. W. J., and J. M. Wallace, 2000: Annular modes in the extratropical circulation. Part I: Month-to-month variability. *J. Climate,* **13,** 1000–1016.

Ting, M., and I. M. Held, 1990: The stationary wave response to a tropical SST anomaly in an idealized GCM. *J. Atmos. Sci.,* **47,** 2546–2566.

Venzke, S., M. R. Allen, R. T. Sutton, and D. P. Rowell, 1999: The atmospheric response over the North Atlantic to decadal changes in sea surface temperature. *J. Climate,* **12,** 2562–2584.

Wallace, J. M., and D. S. Gutzler, 1981: Teleconnections in the geopotential height field during the Northern Hemisphere winter. *Mon. Wea. Rev.,* **109,** 784–812.

Xie, P., and P. A. Arkin, 1997: Global precipitation: A 17-year monthly analysis based on gauge observations, satellite estimates, and numerical model outputs. *Bull. Amer. Meteor. Soc.,* **78,** 2359–2558.